STRUCTURAL CONTROL AND HEALTH MONITORING
Struct. Control Health Monit. 2017;**24**:e1881.
Published online 6 June 2016 in Wiley Online Library (wileyonlinelibrary.com). DOI: 10.1002/stc.1881

Compressive sensing based structural damage detection and localization using theoretical and metaheuristic statistics

Ruigen Yao[1,*,†], Shamim N. Pakzad[1] and Parvathinathan Venkitasubramaniam[2]

[1]*Department of Civil and Environmental Engineering, Lehigh University, Bethlehem, PA 18015, USA*
[2]*Department of Electrical and Computer Engineering, Lehigh University, Bethlehem, PA 18015, USA*

SUMMARY

Accurate structural damage identification calls for dense sensor networks, which are becoming more feasible as the price of electronic sensing systems reduces. To transmit and process data from all nodes of a dense network is a computationally expensive BIG DATA problem; therefore scalable algorithms are needed so that inferences about the current state of the structure can be made efficiently. In this paper, an iterative spatial compressive sensing scheme for damage existence identification and localization is proposed and investigated. At each iteration, damage existence is identified from randomly collected sparse samples and damage localization is iteratively detected via sensing–processing cycles with metaheuristic sampling distribution updating. Specifically, simulated annealing and ant colony analogy are used for guidance in future selection of sensing locations. This framework is subsequently validated by numerical and experimental implementations for gusset plate crack identification.

Received 13 October 2015; Revised 22 February 2016; Accepted 9 April 2016

KEY WORDS: big data; spatial compression; metaheuristics; optimization; statistical hypothesis testing; iterative methods

1. INTRODUCTION

As the technology of structural health monitoring (SHM) matures, sensor networks comprising of a large number of individual sensing channels are becoming more practically and financially feasible [1–5]. In order to transmit and process the large amount of data (BIG DATA) acquired from continuous and/or long-term monitoring, efficient information extraction/compression algorithms in relation to specific structural/site conditions are needed.

Several studies are found in literature that addresses the important problem of structural state information from sensory data (e.g. acceleration, strain, etc.). Among them, global system identification [6–10] employs time and/or frequency analysis for extraction of structural modal properties such as nature frequencies and damping ratios, while other algorithms on a lesser scale attempt to examine certain statistical characteristics of one or several channels of signals to infer the structural condition [11–16]. The information thus acquired can also be used as input for numerical model updating of the original structure [17–20] if high level damage detection is desired.

Traditionally, SHM sensor nodes only perform data collection and transmission: any post-processing and computing of data is done at a central repository that retrieves information from remote nodes. This sensing architecture works well for tethered monitoring systems, where connecting cables serve the dual purpose of information transmission and power supply [21–24]. However, for wireless

*Correspondence to: Ruigen Yao, Department of Civil and Environmental Engineering, Lehigh University, Bethlehem, PA 18015, USA.
†E-mail: yaoruigen@outlook.com

SHM systems [25,26], the transmission cost and energy consumption of centralized data processing becomes inhibitive as the sensor network expands in size [3,27–29]. To overcome this obstacle, decentralized information extraction techniques and communication procedures have been proposed and tried in several studies [30–33], demonstrating increased energy efficiency and better flow of operation.

In the meantime, options to compress the data for wireless transmission are also explored. This can be done by applying the off-the-shelf compression schemes via adaptive coding, and a number of studies that exploit the temporal information redundancy of structural monitoring signals for data condensation are also under way. Examples include compressive sensing from random selection [34–36], sparse matrix representation[37–39], bio-mimicry based signal interpretation [40], and wavelet analysis [41,42]. Such methods reduce the amount of data transmitted per node, yet the central station still needs to communicate directly/indirectly with all sensor nodes within network. But because damage is intrinsically a local phenomenon, even higher performance could be realized if within a dense network only a subset of sensors in the vicinity of possible damage communicates their data with the main repository given proper damage detection features and effective compressive data communication procedures.

In this paper an iterative compact sensing framework on subset identification within dense sensor network for damage detection is introduced. It complements the existing temporal compressive sensing methods, where time histories are compressed at individual sensor nodes. In this scheme, damage existence is first identified via hypothesis testing on the determinant of sample correlation matrix, as a damage feature, among several random locations. Then damage is localized as the location where the maximum Damage Location Indicator (DLI) from iterative random sampling occurs. At each iteration damage indices are computed from the newly drawn random samples, damage location is recognized as that of maximum DLI, and the random sampling distribution is updated according to the accumulated damage indices using either Simulated Annealing [43,44] or Ant Colony Optimization (ACO)[45,46] inspired algorithms. The iteration continues until convergence criteria for the damage location is met.

The organization of the paper is as follows: In Section 2 the complete methodology for damage existence identification and localization using theoretic/metaheuristic statistics is presented. Section 3 details the results from identifying single-point and multi-point damage in a gusset plate simulated in ABAQUS using the nearest-neighbor ratio among strain measurements under uniaxial tension using the proposed methods. Section 4 describes an application of the methods for crack detection in a small scale gusset plate connection under tension test in a laboratory. Conclusion is then drawn on the effectiveness of the compressive sensing (CS) based damage detection framework.

2. METHODOLOGY

This section presents the compressive sensing based damage identification framework. It consists of two stages: damage existence identification from analytical hypothesis testing and damage localization from particle swarm intelligence. Decisions on the structural state are made using data samples from randomly selected sensor subgroups installed on the structure.

2.1. Part I: damage detection using univariate hypothesis testing on several random samples

Hypothesis testing is a statistical tool to identify changes in random sample populations. In the univariate case, its strength is to estimate certain characteristic of the underlying probabilistic distribution from collected samples and compare it to a preset value or threshold calculated either from an assumed theoretical or empirical distribution (known as 'null hypothesis'). Threshold is always associated with a statistical significance level, i.e. the exceeding probability of estimators under the null hypothesis. And when the threshold is exceeded, the hypothesis is rejected and the system properties are deemed changed.

For damage existence detection applications in this paper, structural measurements will be collected continuously from n random locations. Denoting the collected sample vectors as $X_1, X_2, \cdots, X_n$, its

DOI: 10.1002/stc

covariance matrix can be estimated as follows:

$$Cov(X) = 1/NE\Big(\big[X_1 - \overline{X}_{1b}, X_2 - \overline{X}_{2b}, L,\ X_n - \overline{X}_{nb}\big]^T \big[X_1 - \overline{X}_{1b}, X_2 - \overline{X}_{2b}, L,\ X_n - \overline{X}_{nb}\big]\Big) \quad (1)$$

where N is the number of samples taken at each location (thus also the length of each vector). The macron accent $\overline{\{\cdot\}}$ represents the mean of the vector group, and subscript b denotes points from baseline condition. If measurements at these locations are jointly Gaussian random variables, then the covariance estimator follows a Wishart distribution [47]. Statistics based on this assumption can be devised to test whether the mean/variance of the signal vectors has changed simultaneously.

One shortcoming of covariance-based hypothesis testing is that it is affected by excitation or input level. As such, estimated correlation matrix, which is the covariance estimator normalized by the measurement variance at separate locations, is examined instead:

$$\begin{aligned} Corr(X) &= diag([Var(X_1), Var(X_2), L, Var(X_n)])^{-1/2} \\ &*Cov(X)*diag([Var(X_1), Var(X_2), L, Var(X_n)])^{-1/2} \end{aligned} \quad (2)$$

Correlation is robust to input magnitude variation, but its distribution under Gaussian sample assumption is harder to express analytically. Gupta and Nagar [48] provided a formula for computing the probability density function (PDF) of the determinant of the correlation matrix given that the individual variables are uncorrelated:

$$\begin{aligned} f(w) &= c(p,N)w^{-1}\mathrm{G}_{p-1,p-1}^{p-1,0}\left[w\middle|\begin{matrix}\frac{N-1}{2}, \frac{N-1}{2}, L, \frac{N-1}{2} \\ \frac{N-2}{2}, \frac{N-3}{2}, L, \frac{N-p}{2}\end{matrix}\right],\ 0 < w < 1. \\ c(p,N) &= \Gamma^{p-1}\left(\frac{N-1}{2}\right)/\prod_{j=2}^{p}\Gamma\left(\frac{N-j}{2}\right) \\ \mathrm{G}_{p,q}^{m,n}\left[z\middle|\begin{matrix}a_1, L, a_p \\ b_1, L, b_q\end{matrix}\right] &= (2\pi i)^{-1}\int L\left\{\frac{\prod_{j=1}^{m}\Gamma(b_j+h)\prod_{j=1}^{n}\Gamma(1-a_j-h)}{\prod_{j=m+1}^{q}\Gamma(1-b_j-h)\prod_{j=n+1}^{p}\Gamma(a_j+h)}\right\}z^{-h}dh \end{aligned} \quad (3)$$

where p is number of Gaussian random variables, N is the sample size, Γ is the gamma function, and G is the Meijer's G-function as computed by the line integral in complex plane shown in the equation, which is a general expression encompassing many elementary functions such as exponential and logarithmic functions. As measurements happen at individual sensor nodes, it can be assumed that the measurement noise is spatially independent, and this PDF is a fit for jointly testing the statistical properties of measurements at the selected locations. *Left-sided* hypothesis testing will be used here, as when there is a mean drift in the random samples, vectors in Eq. (1) will have stronger correlation, leading to a reduction in correlation determinant value.

2.2. Part II: damage localization using iterative random sampling and statistical inference

The standard damage localization procedure requires effective damage location indices (DLI) to be extracted from collected measurements at different locations. If these damage indices are plotted with respect to their associated locations on the monitored structure, then the peak(s) of this plot will correspond to the damage location(s) (Figure 1).

Data compression schemes generally rely on the assumption that there is redundancy in the full dataset, i.e. knowledge on a selected part of the data will reveal information on the rest. Imagine a DLI field where every value is an independently varying random variable, then even samples from all but one location cannot guarantee the correct detection of maximum peak location—because that last location can either produce the largest peak or not, depending on the realization of the random variable. On the other hand, if the DLI samples demonstrate significant positive correlation among adjacent locations, then significant compression rate might be achieved. As a quick example, assume that a 50 by 50 DLI surface has a single peak that consists of five largest values of the entire group, then a random selection of half of the samples would have more than 97% probability of capturing the 'peak cluster'.

DOI: 10.1002/stc

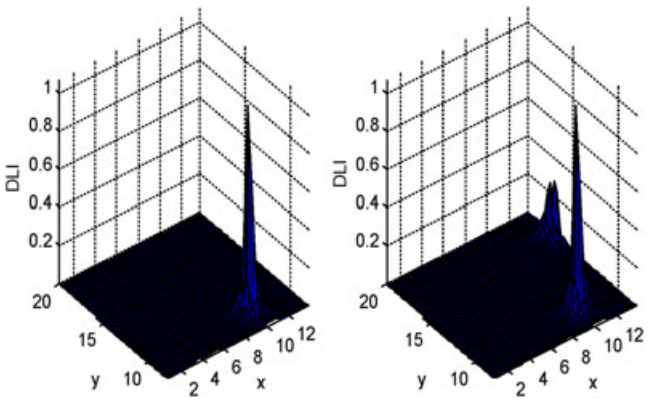

Figure 1. Example of damage location index(DLI) surfaces.

Recognizing that most of the DLIs from structural monitoring applications carry a certain amount of spatial correlation (because the underlying kinematic measurements are correlated), compressive sensing can be applied for savings in data computation and transmission resources. Several key aspects to consider for design of an efficient compact sensing plan are: (i) sampling approach; (ii) adaptation of the sampling scheme based on available measurements; and (iii) the convergence criteria.

Here random compressive sensing using particle swarm intelligence [49–51] will be used because of its agnostic and universal nature. Previous investigations [34–36] on CS showed that signals that can be compressed using classical deterministic methods can also be efficiently acquired from a small set of random measurements. Because of the spatial correlation among DLI samples, partial information on unknown DLI values can be obtained from those collected samples, making the updating of the random sampling probability distribution feasible for enhancing algorithm performance. This process will be carried out in multiple iterations; at each iteration a batch of new DLIs will be added for decision-making (in this context, peak identification). Convergence criteria will be set based on the difference between inference results from consecutive iterations, which reflects the decision error probability.

In the following subsections, two detailed CS procedures, analogous to annealing and ant foraging mechanisms, for DLI will be introduced. While the general principles are based on preexisting literatures on stochastic optimization, the adaptive routines are re-devised and the critical parameters are redesigned to meet the need of data compression.

2.2.1. Simulated annealing-based peak search (SA/PS) algorithm

Annealing is a heat-treatment process commonly adopted in metallurgy to obtain fine quality metals. The guiding concept is to heat the material beyond its critical temperature, then let it cool down gradually such that the molecules will have a higher tendency to form into homogeneous crystal structure instead of irregular coarse grains. Simulated annealing for optimization is first proposed in [43]. It draws inspiration from the statistical mechanics underlying the annealing process, which states that each configuration of the atom system has a probabilistic weight of:

$$\mathrm{W} = \exp(-E\{r_i\}/k_B T). \tag{4}$$

Here $\{r_i\}$ is the set of atomic positions, E stands for state energy, k_B is the Boltzmann's constant, and T is the temperature. In simulated annealing based algorithms, temperature is often assumed to decay exponentially with iteration counts, the energy function equivalent is the cost of each solution, and the transition probability during optimal solution search is:

$$\mathrm{Prob}_{SA} = min\{exp(-\Delta E/k_B T), 1\} \tag{5}$$

where Δ is the difference symbol. This set-up alleviates the danger of the algorithm *getting trapped* at a local optima as a new candidate with a higher cost might still be chosen with a finite probability.

The concept for simulated annealing can be transplanted to the iterative compressive sampling based damage localization problem given that a proper difference energy function is defined. The

DOI: 10.1002/stc

formula adopted for applications in this paper is based on three-sigma rule for Gaussian variables and given as follows:

$$\Delta E = \mathrm{Max}_{\mathrm{avail}}/3\sigma_{\mathrm{avail}} - 1, \tag{6}$$

where the $\mathrm{Max}_{\mathrm{avail}}$ and σ_{avail} are the maximum and standard deviation (without mean removal) of available samples excluding identified peak regions, which are known outliers. k_B is set to 1, while T linearly decreases to zero (termination of algorithm) when half of the points are measured. This exclusion prevents the algorithm from getting stuck around a single peak region. Thus if no new outlier is detected according to the three-sigma rule, uniform random sampling among all unknown locations are adopted; otherwise, the next iteration decides randomly between peak identification or uniform sampling with certain probabilities. The algorithm terminates when the maximum iteration number is reached or three consecutive rounds of uniform random sampling occur. The detailed flow of this algorithm is included in Figure 2.

The process of peak peaking (PP) involves multiple steps/bifurcations in the graph, and thus merits some explanation. The PP algorithm serves two purposes: capturing new peaks in the sensing region, and depicting the surrounding region of outliers ('footprint') of identified peaks. Therefore, the algorithm takes different branches based on comparison between the maximum of the identified peak peripheral(s) and that of the non-peak samples. In case $\mathrm{Max}_{\mathrm{avail}}$ is larger than $\mathrm{Max}(PR_{edge})$ (PR_{edge} is the edge values around peak region) and the former is not a peak, then random sampling is conducted along either the x or y coordinate of $\mathrm{Max}_{\mathrm{avail}}$ in search for a 'section peak' whose x and/or y coordinate will be highly correlated with a 3D peak. The goal here is to detect all significant peaks (thus all damage locations) together with their influence region.

2.2.2. Ant colony optimization based aggregation algorithm (ACO)

Ant is one of the most commonly observed insects that live in highly organized communities. Ant colonies consist of one or more 'queens', a few 'drones', and many 'workers' [52], and are spread around the globe. The ability of adaptation has been attributed to their minute division of duties (reproduction, nesting, foraging for food, etc.) and effective communication among group members.

As part of a larger effort to introduce biological swarm intelligence to the optimization procedures, the ant foraging mechanism has been simulated for a near-optimal solution [53,54].When searching for food, ants leave chemicals (pheromone) along their trails. The more frequent a trail is travelled, the

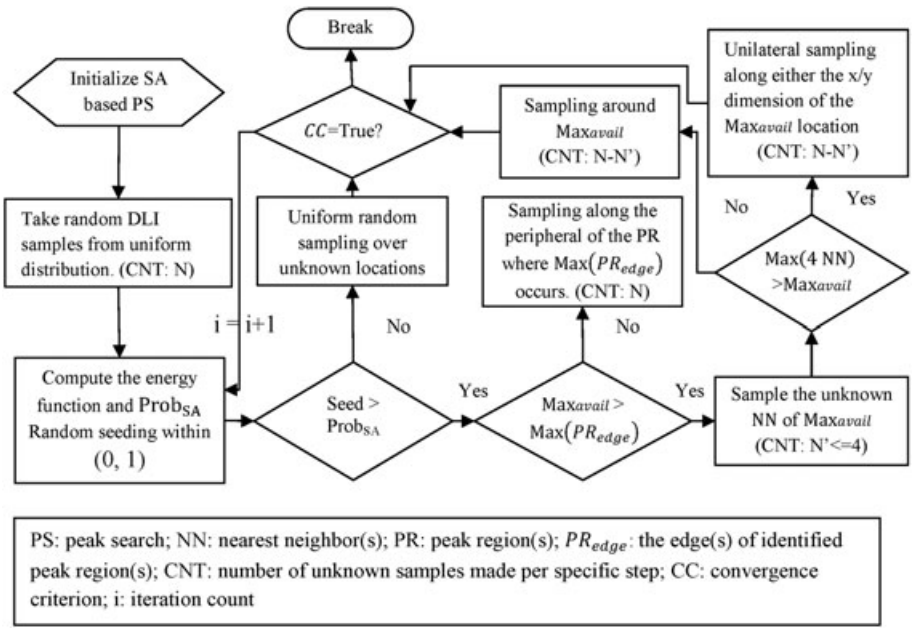

Figure 2. Flow-chart illustration of the SA/PS based damage localization algorithm.

DOI: 10.1002/stc

larger amount of pheromone is deposited on it, which will in turn attract more ants. By simulating this process, optimization algorithms identify those sub-paths that are shared by more explored solutions as more probable components of optimal solutions.

This paper proposes an iterative-compressive-sensing based damage localization, where each ant/agent is a sample made (or to be made) at a location. A batch of 'worker ants' is released every iteration, and their destinations are determined from the current spatial sampling distribution. Initially the distribution is uniform, and routinely updated based on two considerations: (i) the DLI value of the nearest neighbor (from available samples) of each sample location; and (ii) whether the location's nearest neighbor is current and has a higher DLI value than its former nearest neighbor. The first criterion is denoted *desirability* or *sweetness* of a location, while the second criterion is defined its *pheromone* or *potential*. The explicit formulae for desirability, pheromone, and sampling probability computation are shown as below:

$$
\begin{aligned}
Dsrb(x,y)_i &= \begin{cases} 1, \ i=1 \\ DLI\left(NN\left\{[x\ y],[\boldsymbol{x}_{kn}\ \boldsymbol{y}_{kn}]_i\right\}\right), \ i>1 \end{cases} \\
Pher(x,y)_i &= \begin{cases} 1, \ i\le 2 \\ [0.9+0.1 logical\left(NN\left\{[x\ y],[\boldsymbol{x}_{kn}\ \boldsymbol{y}_{kn}]_{i-1}\right\} == NN\left\{[x\ y],[\boldsymbol{x}_{kn}\ \boldsymbol{y}_{kn}]_i\right\}\right) \\ +0.2 logical\left(Dsrb(x,y)_i > Dsrb\left(NN\left\{[x\ y],[\boldsymbol{x}_{kn}\ \boldsymbol{y}_{kn}]_i\right\}\right)_{i-1}\right)]Pher(x,y)_{i-1}, \ i>2 \end{cases} \\
p(x,y)_i &= \begin{cases} 0, \ [x\ y]\in[\boldsymbol{x}_{kn}\ \boldsymbol{y}_{kn}]_i \\ \dfrac{Pher(x,y)_i \cdot Dsrb(x,y)_i}{\sum_{[x\ y]\notin[\boldsymbol{x}_{kn}\ \boldsymbol{y}_{kn}]_i} Pher(x,y)_i \cdot Dsrb(x,y)_i}, \ [x\ y]\notin[\boldsymbol{x}_{kn}\ \boldsymbol{y}_{kn}]_i \end{cases}
\end{aligned}
\tag{7}
$$

Here subscript i denotes the iteration number, subscript 'kn' stands for 'known', and $NN\{set1, set2\}$ is the operation of finding the nearest neighbors of $set1$ in $set2$. Note $[\boldsymbol{x}_{kn}\ \boldsymbol{y}_{kn}]_i$ refers to the collection of known samples prior to ith round of sampling. Thus here the desirability function is Voronoi tessellation result over the sensing region about currently available DLIs, and the pheromone is only updated at locations within Voronoi cells associated with DLIs from the latest round of sampling, where the values are multiplied by 1.1 if desirability increase, and 0.9 if otherwise [55]. The search stops either after a preset number of iteration (N_{iter}) or after the variation of the 'pheromone' or 'potential' map becomes negligible and stable:

$$
\begin{aligned}
CC = i \ge N_{iter} P\Bigg(&\left\{\left|1-\frac{|Pher_i|}{|Pher_{i-1}|}\right| < 5\%\right\} \&\& \left\{\left|1-\frac{|Pher_{i-1}|}{|Pher_{i-2}|}\right| < 5\%\right\} \\
&\&\&\{(Pher_i - Pher_{i-1})(Pher_{i-1} - Pher_{i-2}) < 0\}\Bigg).
\end{aligned}
\tag{8}
$$

The *negligibility* requirement here is expressed as the incremental normalized difference of pheromone within 5% for two consecutive times, while the *stability* requirement is evinced as a sign change in the difference. The detailed flow chart of this CS scheme is presented in Figure 3.

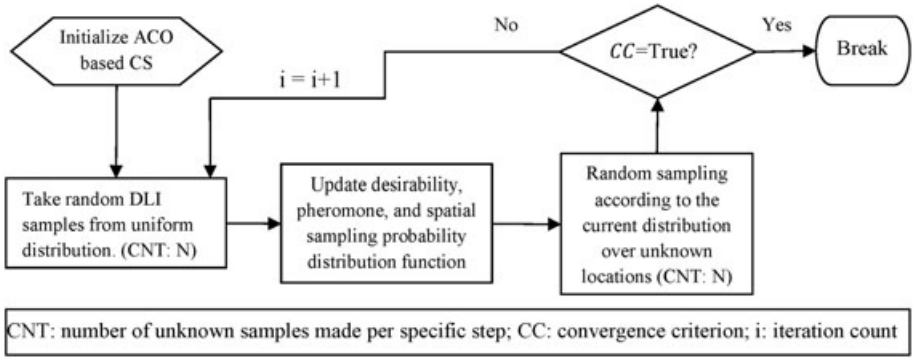

Figure 3. Flow-chart illustration of the ACO inspired damage localization algorithm.

DOI: 10.1002/stc

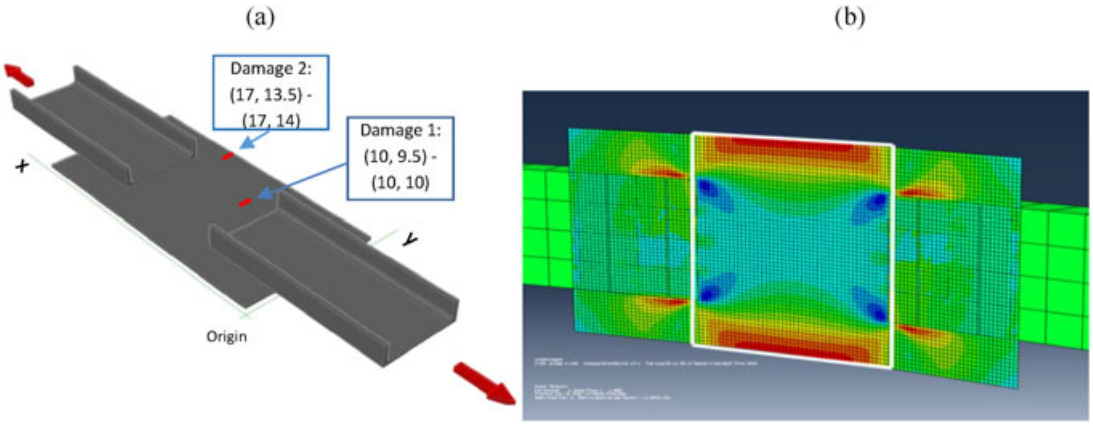

Figure 4. (a) Simulation/Test Setup; (b) close-up of the undamaged gusset-plate in ABAQUS.

The framework of these two metaheuristic methods is advantageous in that they do not rely on assumptions on DLI surface forms and thus adapt to different possible damage scenarios. In the subsequent section, they will be validated through a simulation example.

The above two metaheuristic damage localization schemes, although distinct in details, both borrow from subspace-driven optimization literature, which focuses on the problem of getting a near-optimal result by randomly searching the solution space. According to the definition of DLI, damage localization is essentially a peak(s) depiction application. Thus if the DLI surface over sensing region is considered equivalent of the objective function for an optimization problem and every location a solution, one can naturally form analogies between the iterative compressive sensing methods and optimization techniques.

3. NUMERICAL VALIDATION

To evaluate the effectiveness of the proposed damage existence detection and localization algorithms, they are applied to detect damage in a two-way gusset plate connection (Figure 4a) simulated in ABAQUS using shell elements. The connection is set under uniform tension from both sides.

The specimen was composed of two C8x11.5 channel members welded (simulated by tie constraints) to a 14 × 28 inch plate that had a thickness of ¼ inch. Each of the connecting members was 20 inches long and has 8-inch overlap with the main plate. The locations of damage on the plate occur in the middle portion of the plate that is left free of connections to allow ease of data analysis. The assembled connection was 52 inches in length and was designed to withstand up to 100 kips of axial tensile force.

The simulation consisted of three stages: (i) the plate was undamaged, providing control readings of strain with which to compare the results of the subsequent stages; (ii) a crack was made from coordinate (10, 10) to coordinate (10, 9.5); (iii) another crack was added on the edge of the plate from coordinate (17,13.5) to coordinate (17,14). Cracks on the plate were simulated using the 'SEAM' option. The (x,y) coordinate system and damage locations are illustrated in Figure 4a.

Nodal train data from the plate was acquired for use as input for the calculation of the damage indices and for the iterative sampling scheme. Figure 4b shows the strain on the plate at Stage 1. The adopted element size is 0.25 inch, and the outlined area defines the 12 × 14 inch range of data used later for the sampling scheme.

Table I. Hypothesis testing results on measurement correlation matrix for the simulation. $N = 50$, $p = 10$.

	Stage 1	Stage 2	Stage 3
$\mathrm{Det}(\hat{Corr})$	0.3561	0.2632	0.2703
$Prob(\mathrm{Det}(Corr) < \mathrm{Det}(\hat{Corr}))$	0.4127	0.0441	0.0600

DOI: 10.1002/stc

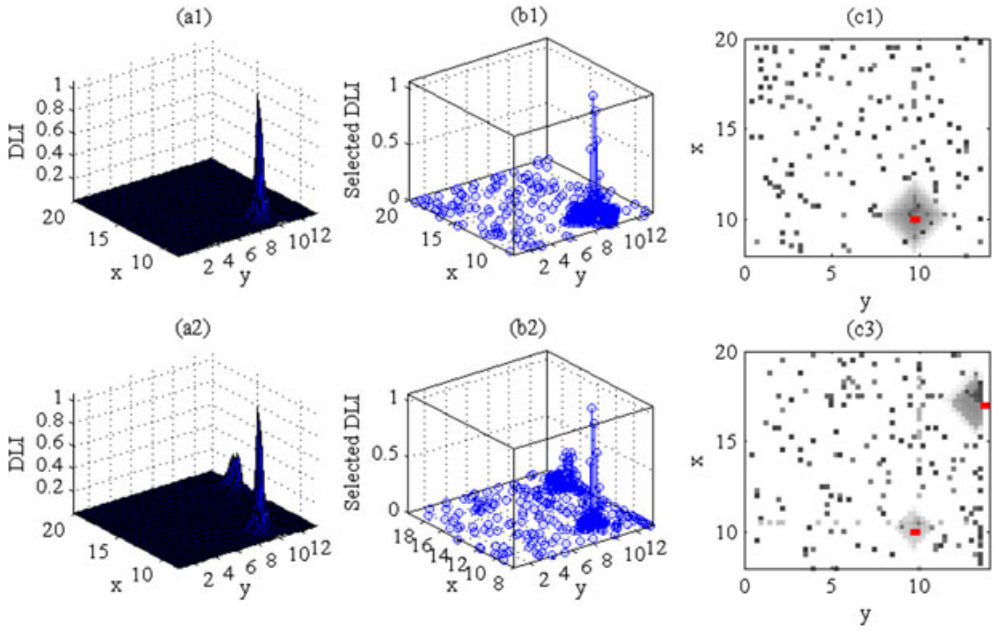

Figure 5. Iterative CS based damage localization from SA/PS algorithm. First row and second row are about Damage State 1 and 2, respectively. (a1)–(a2): the complete set of DLIs over the monitored surface; (b1)–(b2): samples from CS; (c1)–(c2): plane view of the sensing/damage locations (darker hue represents higher iteration order).

Table I shows the hypothesis testing results out of three datasets obtained respectively from three structural conditions. Random noise at 5% level is added to the original static strain to create multiple measurements. The metric presented here is the exceeding probability corresponding to the correlation determinant calculated from measurements at six randomly selected locations. It can be seen that as the system becomes damaged, the exceeding probability reduces drastically, signaling a statistically significant change.

Damage localization result from SA/PS method is given in Figure 5, and the key CS metrics are listed in Table II. Initial temperature (Parameter adopted in Eq. (5)) for this search is set at 80. Assuming decentralized DLI computation, the spatial sampling is performed directly on the damage location indicators, which is defined as the average of the correlation coefficients between the strain measured at current location and each of the nearest neighbor locations in this application. Even though compressive sensing uses only a fraction of the DLIs over the total sensing region, it very well characterizes the DLI 'peak regions' for both single and two-point damage cases, and thus conveys most of the information pertaining to structural damage properties. The algorithm stopped after 22 rounds of iteration is completed: Figure 5 (c1) and (c2) show that for both damage cases, the crack *footprint*(*s*) is very finely sampled in the middle of the process, and samples from last rounds of iteration are scattered over entire area.

Results from ACO based damage location search is presented in Figure 6. The algorithm was set to run for 16 iterations; however, it ended the search early after the 13th iteration as the detected variation of pheromone map becomes sufficiently small. The algorithm is able to achieve better compression (i.e. fewer locations to retrieve data) than the SA alternative, but at the same time,

Table II. Some parameters of CS based damage localization set-up and results for the simulation.

	Total no. of iterations	No. of samples per iteration	Local peak captured?	CS rate (no. of CS samples / no. of total samples)
SA/PS algorithm	22	14	Y/(Y Y)	11.86%
ACO algorithm	13	12	Y/(Y Y)	6.01%

DOI: 10.1002/stc

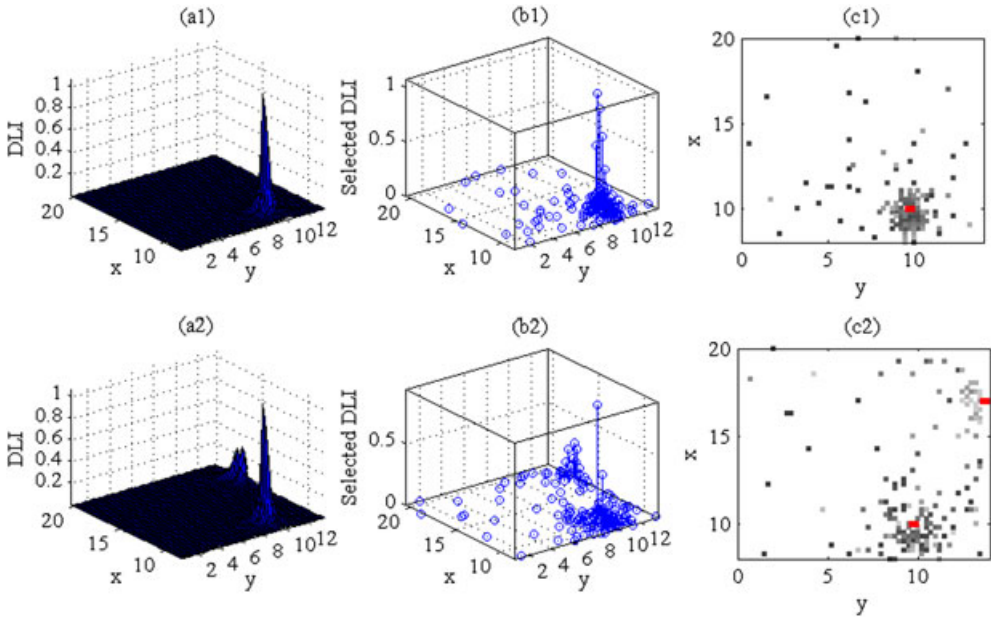

Figure 6. Iterative CS based damage localization from ACO algorithm. First row and second row are about Damage State 1 and 2, respectively. (a1)–(a2): the complete set of DLIs over the monitored surface; (b1)–(b2): samples from CS; (c1)–(c2): plane view of the sensing/damage locations (darker hue represents higher iteration order).

the peak regions are not so well depicted because the ant colony analogy comes with more flexibility than greedy peak search. Also, at later stages of iterative CS, major portion of the samples are far from peak regions.

The results show that both algorithms are effective CS based damage localization options, with the SA/PS algorithm better at depicting the damage affected region, and the ACO algorithm an enhanced compression performance. The CS algorithms come with a set of parameters (e.g. nominal temperature control scheme for SA, pheromone updating coefficients for ACO, and samples per iteration for both) that can be adjusted based on different applications to optimize performance.

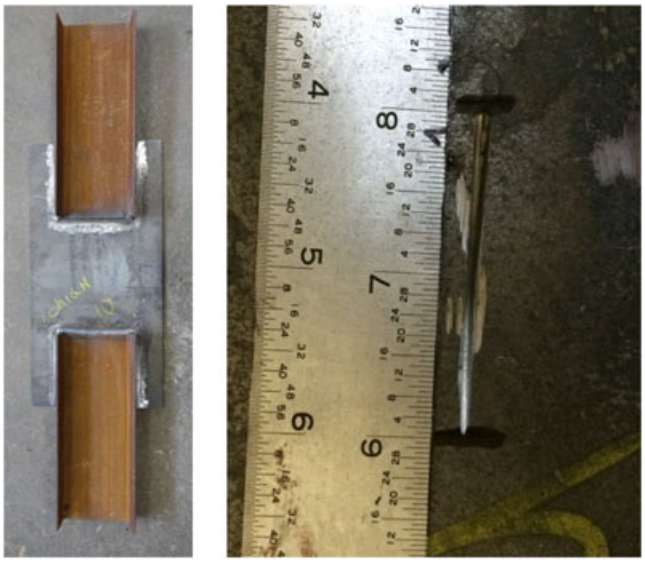

Figure 7. The Gusset Plate Connection constructed in Lab (Left) and the artificial damage site (Right).

DOI: 10.1002/stc

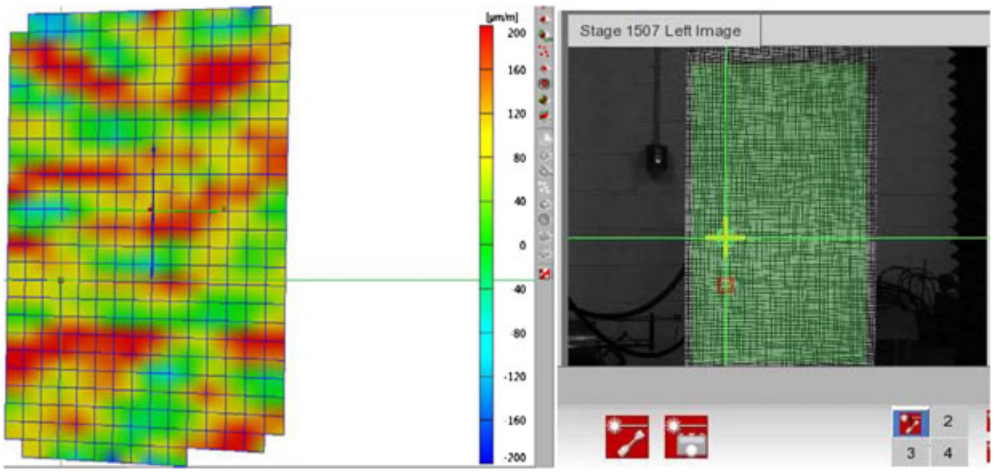

Figure 8. Close-up of the Aramis DIC system interface: Left: strain color plot of the plate under full load; Right: calibration picture of the gusset plate from left camera.

4. EXPERIMENTAL VALIDATION

For further validation of the proposed damage existence identification and localization algorithms, a physical experiment was conducted in the ATLSS laboratory using the SATEC 600kip Hydraulic Testing System for a scaled gusset plate connection (Figure 7). Axial tensile forces were placed on the specimen (size of the specimen is the same as the simulated example) while using the Aramis DIC system to monitor the change in the in-plane strain field on the specimen during the different stages of damage. The sensing point grid formed in DIC system (Figure 8) is treated as a dense sensor network here.

The measurement origin is defined at the center of the plate. Damage is created as a grinded dent (Figure 7) on the back side from location (−3.25, −3.5) to (−3.25, −2.25) (unit: inches). For both the damaged and undamaged state, the plate is gradually loaded to 20 kips, and unloaded to zero. One thousand pictures are taken by the DIC system when the plate is fully loaded for each state.

An investigation of the strain contour plot over the plate surface reveals that strain distribution has erratic high and low stress concentrations scattered around. This could partially be attributed to the system inaccuracies of DIC, which does not yield accurate measurements for values smaller than 100 micro strain (this is more than half of the average measured strain in the plate). Besides, environmental uncertainties (change of lighting etc.) cause oscillation in measurement sequences and the mensuration quality degrades along the plate edges. Thus although a large number of pictures are taken, the estimated DLI surface is still noisy, which adversely affect the compressive sensing outcome to a significant degree.

In the same format as the simulation section, hypothesis testing for damage existence identification results is shown in Table III. Figures 9 and 10 show the CS results on two DLIs using the SA/PS and ACO algorithms, with Table IV displaying key CS metrics. The *first* DLI is the relative difference in the average correlation coefficients between measurements at a sensor and those at its nearest neighbors, while the *second* DLI is the strain difference between damaged and undamaged stages normalized by the respective measurement standard deviations at respective sensing locations. It is found that the first DLI, instead of capturing the damage location, peaks at zero-crossing parts of strain contour. The second DLI identifies the horizontal location of the dent in form of a long ridge at the lower left of the plate surface around 3.3 inches below the x axis. Both algorithms detect the regions

Table III. Hypothesis testing results on measurement correlation matrix for the experiment. $N = 50$, $p = 5$.

	Stage 1	Stage 2
$\mathrm{Det}(\hat{Corr})$	0.7840	0.0082
$Prob(\mathrm{Det}(Corr) < \mathrm{Det}(\hat{Corr}))$	0.3360	0.0000

DOI: 10.1002/stc

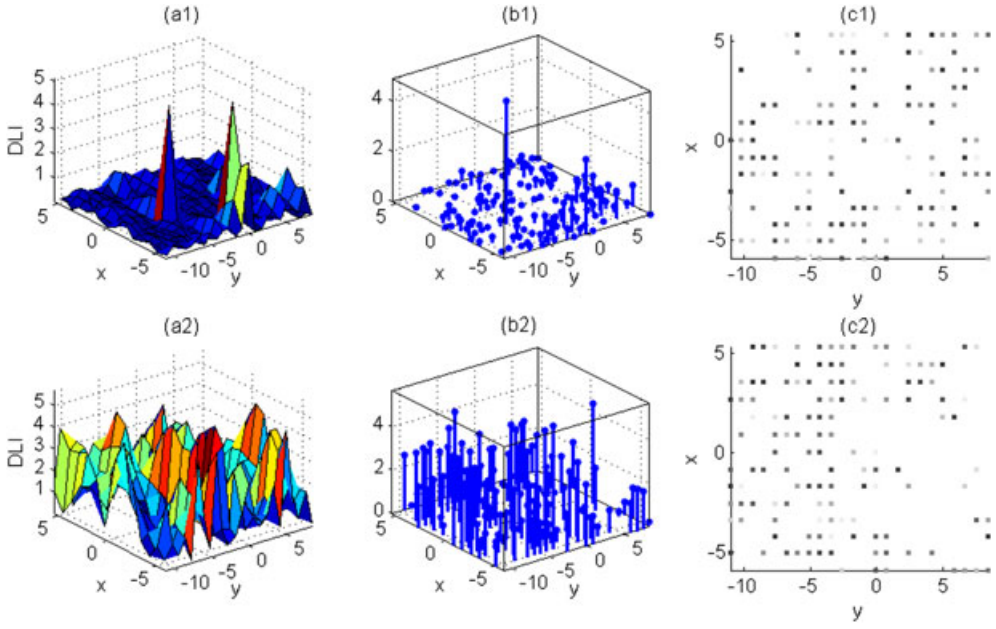

Figure 9. Iterative CS based damage localization from SA/PS algorithm for the laboratory gusset plate connection. first row and second row are for DLI 1 and 2, respectively. (a1)–(a2): the complete set of DLIs over the monitored surface; (b1)–(b2): samples from CS; (c1)–(c2): plane view of the sensing/damage locations (darker hue represents higher iteration order).

of interest using a subset of DLIs. The CS rate here is much larger than those in the simulation example as the algorithms have to filter away many noisy peaks within the region to identify the features of significance.

The experimental results are presented as support of the effectiveness of algorithms particularly for damage existence identification under low-sensing resolution conditions. Because of the large variation/bias of data, DLI surfaces for this experiment show spurious creases, which complicate

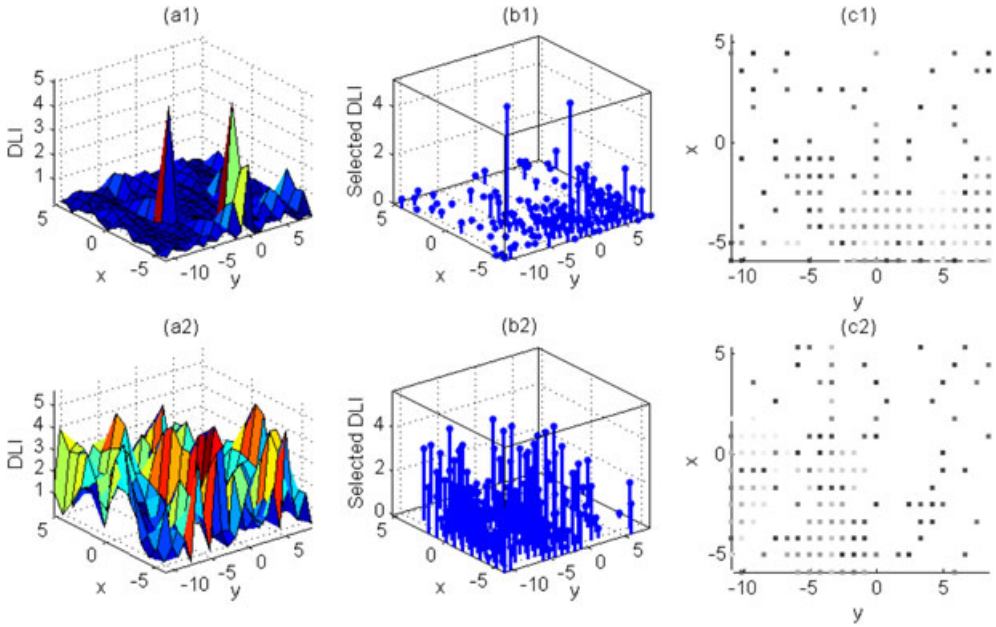

Figure 10. Iterative CS based damage localization from ACO algorithm for the laboratory gusset plate connection. First row and second row are for DLI 1 and 2, respectively. (a1)–(a2): the complete set of DLIs over the monitored surface; (b1)–(b2): samples from CS; (c1)–(c2): plane view of the sensing/damage locations (darker hue represents higher iteration order).

DOI: 10.1002/stc

Table IV. Some parameters of CS based damage localization set-up and results for the experiment.

	Total no. of iterations	No. of samples per iteration	Critical region captured?	CS rate (no. of CS samples / no. of total samples)
SA/PS algorithm	18	8	Y, Y	42.86%
ACO algorithm	17	8	Y, Y	40.48%

detection procedure considering the underlying assumption that DLIs in close neighborhoods are positively correlated. Thus the suboptimal performance here is because of inaccurate DLIs estimation and insufficient signal to noise ratio, rather than from algorithm inefficiencies.

5. CONCLUSION

In this paper, a damage existence identification and localization strategy based on compact sensing of dense sensor network(s) is outlined. Existence identification of damage is accomplished via theoretical hypothesis testing on the spatial correlation matrix of randomly collected samples, and if a change is thus detected, localization is performed using selective sensor 'sampling'. The sampling distribution is routinely updated on incoming sensor measurements through SA/PS and ACO inspired optimization algorithm, which helps the selection to converge to the true damage location after a few rounds of measurement retrieval at random sensor locations. This framework is validated through both numerical and experimental implementations.

When performing hypothesis testing on determinant of the correlation matrix, careful consideration should be paid to the choice of number of spatial locations and samples collected overtime. It is beneficial to collect many measurements per node when possible (especially when many sensing locations are included), so that the correlation matrix is less likely to demonstrate significant off-diagonal terms at baseline state, and the normality assumption of data would cause less modeling error.

Note that both SA/PS and ACO damage localization algorithms presented here are based on the assumption that there is positive spatial correlation among DLIs at different sensing locations; the more prominent this correlation is, the more significant compression can be achieved. This is validated by the observation that smaller amount of samples is needed to locate damage in the numerical implementation, where the DLI peaks are well defined, than that in the experimental implementation, where the DLI values exhibit random fluctuations over the sensing region.

In another perspective, the idea of iterative subspace sampling based damage detection is to decrease the number of sensors needed to transmit data at the expense of increased computation activity in the base station. This exchange could lead to total energy savings and improvement of the flow of sensing/control for SHM, especially when wireless sensors are involved.

To sum up, the two-step damage detection methodology is shown to be successful in the simulation application presented herein. Correlation matrix testing is a straightforward way to capture structural change, while the metaheuristics-inspired damage localization procedure is very flexible and can adapt to different damage forms. This set of methods will be further tried out in a variety of situations (probably on full scale structures) for better assessment of their performance, and also for determination of optimal parameter sets for the damage localization in different conditions.

ACKNOWLEDGEMENTS

Research funding is partially provided by the National Science Foundation through Grant No. CMMI-1351537 by Hazard Mitigation and Structural Engineering program, and by a grant from the Commonwealth of Pennsylvania, Department of Community and Economic Development, through the Pennsylvania Infrastructure Technology Alliance (PITA).

DOI: 10.1002/stc

REFERENCES

1. Lynch J, Loh K. A summary review of wireless sensors and sensor networks for structural health monitoring. *Shock and Vibration Digest* 2006; **38**(91):91–128.
2. Farrar CR, Park G, Allen DW, Todd MD. Sensor network paradigms for structural health monitoring. *Structural Control and Health Monitoring* 2006; **13**(1):210–225.
3. Pakzad S. Development and deployment of large scale wireless sensor network on a long-span bridge. *Smart Structures and Systems* 2010; **6**(5–6):525–543.
4. Cheng L, Pakzad SN. 2009. Agility of wireless sensor networks for earthquake monitoring of bridges. 2009 Sixth International Conference on Networked Sensing Systems (INSS), IEEE, pp. 1–4.
5. Lan C, Zhou Z, Ou J. Monitoring of structural prestress loss in RC beams by inner distributed Brillouin and fiber Bragg grating sensors on a single optical fiber. *Structural Control and Health Monitoring* 2014; **21**(3):317–330.
6. Ljung L. System Identification: Theory for the User. Information and System Sciences Series. Prentice-Hall: Englewood Cliffs, NJ, 1987.
7. Alvin KF, Robertson AN, Reich GW, Park KC. Structural system identification: from reality to models. *Computers & Structures* 2003; **81**(12):1149–1176.
8. Pakzad SN, Rocha GV, Yu B. Distributed modal identification using restricted auto regressive models. *International Journal of Systems Science* 2011; **42**(9):1473–1489.
9. Peeters B, Ventura CE. Comparative study of modal analysis techniques for bridge dynamic characteristics. *Mechanical Systems and Signal Processing* 2003; **17**(5):965–988.
10. Chang M, Pakzad S. Modified natural excitation technique for stochastic modal identification. *Journal of Structural Engineering* 2012; **139**(10):1753–1762.
11. Sohn H, Farrar CR, Hunter NF, Worden K. Structural health monitoring using statistical pattern recognition techniques. *Journal of Dynamic Systems, Measurement, and Control* 2001; **123**(4):706–711.
12. Nair K, Kiremidjian A, Law K. Time series-based damage detection and localization algorithm with application to the ASCE benchmark structure. *Journal of Sound and Vibration* 2006; **291**(1–2):349–368.
13. Yao R, Pakzad SN. Autoregressive statistical pattern recognition algorithms for damage detection in civil structures. *Mechanical Systems and Signal Processing* 2012; **31**:355–368.
14. de Lautour OR, Omenzetter P. Nearest neighbor and learning vector quantization classification for damage detection using time series analysis. *Structural Control and Health Monitoring* 2010; **17**(6):614–631.
15. Yao R, Pakzad SN. Damage and noise sensitivity evaluation of autoregressive features extracted from structure vibration. *Smart Materials and Structures* 2014; **23**(2):025007.
16. Shahidi SG, Nigro MB, Pakzad SN, Pan Y. Structural damage detection and localisation using multivariate regression models and two-sample control statistics. *Structure and Infrastructure Engineering* 2015; **11**(10):1277–1293.
17. Weber B, Paultre P. Damage identification in a truss tower by regularized model updating. *Journal of Structural Engineering* 2010; **136**(3):307–316.
18. Shahidi SG, Pakzad SN. Generalized response surface model updating using time domain data. *Journal of Structural Engineering* 2014; **140**(8):A4014001.
19. Friswell M, Mottershead J. Finite Element Model Updating in Structural Dynamics. Springer: Berlin, 1995.
20. Brownjohn J, Xia P, Hao H, Xia Y. Civil structure condition assessment by FE model updating: methodology and case studies. *Finite Elements in Analysis and Design* 2001; **37**(10):761–775.
21. Dorvash S, Pakzad S, Labuz E. Statistics based localized damage detection using vibration response. *Smart Structures and Systems* 2014; **14**(2):85–104. DOI: http://dx.doi.org/10.12989/sss.2014.14.2.085
22. Gul M, Catbas FN. Statistical pattern recognition for Structural Health Monitoring using time series modeling: theory and experimental verifications. *Mechanical Systems and Signal Processing* 2009; **23**(7):2192–2204.
23. Celebi M. 2002. Seismic instrumentation of buildings (with emphasis on federal buildings). Special GSA/USGS Project, an administrative report.
24. Farrar CR, Baker WE, Bell TM, Cone KM, Darling TW, Duffey TA, Eklund A, Migliori A. 1994. Dynamic characterization and damage detection in the I-40 bridge over the Rio Grande, Los Alamos, NM.
25. Kling R, Adler R, Huang J, Hummel V, Nachman L. Intel Mote-based sensor networks. *Structural Control and Health Monitoring* 2005; **12**(3–4):469–479.
26. Chen Z, Casciati F. A low-noise, real-time, wireless data acquisition system for structural monitoring applications. *Structural Control and Health Monitoring* 2014; **21**(7):1118–1136.
27. Lynch JP. An overview of wireless structural health monitoring for civil structures. *Philosophical Transactions. Series A, Mathematical, Physical, and Engineering Sciences* 2007; **365**(1851):345–72.
28. Wang Y, Lynch JP, Law KH. A wireless structural health monitoring system with multithreaded sensing devices: design and validation. *Structure and Infrastructure Engineering* 2007; **3**(2):103–120.
29. Xu N, Rangwala S, Chintalapudi K, Ganesan D, Broad A, Govindan R, Estrin D. 2004. A wireless sensor network for structural monitoring. Center for Embedded Network Sensing.
30. Rice JA, Spencer Jr., BF. 2008. Structural health monitoring sensor development for the Imote2 platform. Proceedings of the SPIE—The International Society for Optical Engineering, SPIE—The International Society for Optical Engineering, pp. 693231–693234.
31. Kim S, Pakzad S, Culler D, Demmel J, Fenves G, Glaser S, Turon M. 2007. Health monitoring of civil infrastructures using wireless sensor networks. Information Processing in Sensor Networks, 2007. IPSN 2007. 6th International Symposium on, Cambridge, MA, pp. 254–263.
32. Li X, Dorvash S, Cheng L, Pakzad S. 2011. An implementation of a data-transmission pipelining algorithm on Imote2 platforms. SPIE Smart Structures and Materials + Nondestructive Evaluation and Health Monitoring, M. Tomizuka, ed., International Society for Optics and Photonics, pp. 798104–798104–7.
33. Tanner NA, Wait JR, Farrar CR, Sohn H. Structural health monitoring using modular wireless sensors. *Journal of Intelligent Materials Systems and Structures* 2003; **14**(1):43–56.

34. O'Connor SM, Lynch JP, Gilbert AC. Compressed sensing embedded in an operational wireless sensor network to achieve energy efficiency in long-term monitoring applications. *Smart Materials and Structures* 2014; **23**(8):085014.
35. Bao Y, Beck JL, Li H. Compressive sampling for accelerometer signals in structural health monitoring. *Structural Health Monitoring* 2010; **10**(3):235–246.
36. Mascarenas D, Cattaneo A, Theiler J, Farrar C. Compressed sensing techniques for detecting damage in structures. *Structural Health Monitoring* 2013; **12**(4):325–338.
37. Wang Z, Chen G. A moving-window least squares fitting method for crack detection and rigidity identification of multispan bridges. *Structural Control and Health Monitoring* 2013; **20**(3):387–404.
38. Balsamo L, Betti R. Data-based structural health monitoring using small training data sets. *Structural Control and Health Monitoring* 2015; **22**(10):1240–1264.
39. Yang Y, Nagarajaiah S, Ni Y-Q. Data compression of very large-scale structural seismic and typhoon responses by low-rank representation with matrix reshape. *Structural Control and Health Monitoring* 2015; **22**(8):1119–1131.
40. Peckens CA, Lynch JP. Utilizing the cochlea as a bio-inspired compressive sensing technique. *Smart Materials and Structures* 2013; **22**(10):105027.
41. Zhang Y, Li J. Wavelet-based vibration sensor data compression technique for civil infrastructure condition monitoring. *Journal of Computing in Civil Engineering* 2006; **20**(6):390–399.
42. Ji S, Huang L, Wang J, Shen J. The application of wavelet threshold on compressive sensing in wireless sensor networks. *International Journal of Hybrid Information Technology* 2014; **7**(1):225–232.
43. Kirkpatrick S, Gelatt C Jr, Vecchi M, McCoy A. Optimization by simulated annealing. *Science, New Series* 1983; **220** (4598):671–680.
44. Zimmerman AT, Lynch JP, Ferrese FT. Market-based resource allocation for distributed data processing in wireless sensor networks. *ACM Transactions on Embedded Computing Systems* 2013; **12**(3):1–28.
45. Dorigo M, Birattari M. 2010. Ant colony optimization. Encyclopedia of Machine Learning.
46. Putha R, Quadrifoglio L, Zechman E. Comparing ant colony optimization and genetic algorithm approaches for solving traffic signal coordination under oversaturation conditions. *Computer-Aided Civil and Infrastructure Engineering* 2012; **27**(1):14–28.
47. Conradsen K, Nielsen AA, Schou J, Skriver H. A test statistic in the complex wishart distribution and its application to change detection in polarimetric SAR data. *IEEE Transactions on Geoscience and Remote Sensing* 2003; **41**(1):4–19.
48. Gupta A, Nagar D. Distribution of the determinant of the sample correlation matrix from a mixture normal model. *Random Operators and Stochastic Equations* 2004; **12**(2):193–199.
49. Zhong G, Kobayashi Y, Emaru T, Hoshino Y. Approaches based on particle swarm optimization for problems of vibration reduction of suspended mobile robot with a manipulator. *Journal of Vibration and Control* 2012; **20**(1):3–23.
50. Zhan D, Lu H, Hao W, Jin D. Improving particle swarm optimization: using neighbor heuristic and Gaussian cloud learning. *Intelligent Data Analysis* 2016; **20**(1):167–182.
51. Steele JC, Mahoney K, Karovic O, Mays LW. 2016. Heuristic optimization model for the optimal layout and pipe design of sewer systems. Water Resources Management.
52. Dorigo M, Birattari M, Stutzle T. 2006. Ant colony optimization. Computational Intelligence Magazine, IEEE.
53. Putha R. 2012. Comparing ant colony optimization and genetic algorithm approaches for solving traffic signal coordination under oversaturation conditions. Computer-Aided Civil and Infrastructure Engineering.
54. Alaya I, Solnon C, Ghedira K. 2007. Ant colony optimization for multi-objective optimization problems. 19th IEEE International Conference on Tools with Artificial Intelligence(ICTAI 2007), IEEE, pp. 450–457.
55. Aurenhammer F. Voronoi diagrams—a survey of a fundamental geometric data structure. *ACM Computing Surveys* 1991; **23**(3):345–405.

DOI: 10.1002/stc